The Astrophysical Journal, 625:L75–L78, 2005 June 1

THE DETECTION OF SILICATE EMISSION FROM QUASARS AT 10 AND 18 MICRONS

Lei Hao,[1] H. W. W. Spoon,[1,2] G. C. Sloan,[1] J. A. Marshall,[1] L. Armus,[3] A. G. G. M. Tielens,[4] B. Sargent,[5] I. M. van Bemmel,[6] V. Charmandaris,[1,7,8] D. W. Weedman, and [1] J. R. Houck[1]

Received 2005 March 24; accepted 2005 April 19; published 2005 May 10

ABSTRACT

We report the spectroscopic detection of silicate emission at 10 and 18 μm in five PG quasars, the first detection of these two features in galaxies outside the Local Group. This finding is consistent with the unification model for active galactic nuclei (AGNs), which predicts that an AGN torus seen pole-on should show a silicate emission feature in the mid-infrared. The strengths of the detected silicate emission features range from 0.12 to 1.25 times the continuum at 10 μm and from 0.20 to 0.79 times the continuum at 18 μm. The silicate grain temperatures inferred from the ratio of 18 μm to 10 μm silicate features under the assumption of optically thin emission range from 140 to 220 K.

Subject headings: galaxies: active — galaxies: ISM — infrared: galaxies — quasars: emission lines

1. INTRODUCTION

Active galactic nuclei (AGNs) are broadly classified in two types: type 1 AGNs, which display broad hydrogen emission lines in the optical, and type 2 AGNs, which do not. The AGN unification model (e.g., Antonucci 1993) ties these two types together. An optically and geometrically thick dusty torus surrounds a central black hole, accretion disk, and broad-line emission region. Sources viewed face-on are recognized as type 1, while edge-on sources are type 2. Observations at many wavelengths support this scenario (e.g., Antonucci & Miller 1985), but until now there was a lack of constraining data in the mid-infrared.

Silicate dust is a major component of the interstellar medium in the Milky Way and other galaxies. It produces two spectral features in the infrared: a "10 μm feature" that arises from a Si−O stretching mode, and an "18 μm feature" from an O−Si−O bending mode (e.g., Knacke & Thomson 1973). Emission or absorption from silicate dust is a dominant feature of the infrared spectrum produced by most mass-losing evolved stars, interstellar clouds, H II regions, and circumstellar disks around young stellar objects. Silicate absorption is also detected in dusty starburst galaxies (Rigopoulou et al. 1999), ultraluminous infrared galaxies (ULIRGs; Genzel et al. 1998; Tran et al. 2001; Spoon et al. 2004; Armus et al. 2004), and a sample of mid-infrared detected, optically invisible, high-luminosity galaxies with redshifts of $1.7 < z < 2.8$ (Houck et al. 2005).

Type 2 AGNs show silicate dust in absorption as expected, but the mid-infrared spectroscopic data for type 1 AGNs have been scarce. Recently, Siebenmorgen et al. (2005) presented spectra of two quasars with just the 10 μm feature in emission. While radiative transfer models clearly predict silicates to be in emission for type 1 sources (Laor & Draine 1993; Pier & Krolik 1992, 1993; Granato & Danese 1994; Efstathiou & Rowan-Robinson 1995; Nenkova et al. 2000, 2001, 2002; van Bemmel & Dullemond 2003; Dullemond & van Bemmel 2005), the absence of the silicate emission features at 10 and 18 μm has led to models without strong silicate emission. Laor & Draine (1993) and van Bemmel & Dullemond (2003) have suggested that larger grains dominate the grain-size distribution. Nenkova et al. (2002) instead proposed that if the torus is clumpy, the 10 μm silicate emission can be sufficiently suppressed, although Dullemond & van Bemmel (2005) have challenged this suggestion.

Here we report the first spectroscopic detection of both silicate features at high signal-to-noise ratios in five PG quasars. Quasars are the high-luminosity counterparts of Seyfert 1 galaxies, showing the same broad emission lines that define type 1 AGNs.

2. OBSERVATIONS AND DATA REDUCTION

The five sources presented in this Letter (PG 0804+761, PG 1211+143, PG 1351+640, I Zw 1 [=PG 0050+124], and 3C 273 [=PG 1226+023]) were selected from a sample of 12 AGNs, based on their prominent silicate emission features at both 10 and 18 μm. The observations were part of the Guaranteed Time Observation program of the Infrared Spectrograph[9] (IRS; Houck et al. 2004) on the *Spitzer Space Telescope* (Werner et al. 2004). Table 1 lists the basic properties of these targets, along with their observation dates and on-source integration times. All of them have broad Hβ lines (Boroson & Green 1992) and therefore are classified as type 1 AGNs. Two of them, 3C 273 and PG 1211, are radio-loud quasars, and the rest are radio-quiet (Sanders et al. 1989). All five quasars are very luminous, as can be seen from the bolometric luminosities in Table 1 (from Sanders et al. 1989).

The observations were made with the Short-Low (SL) and Long-Low (LL) modules of the IRS. The spectra were extracted from the flat-fielded images provided by the *Spitzer* Science Center (pipeline ver. S11.0.2). The images were background-subtracted by differencing the two SL apertures, and by differencing the two nod positions for LL. Spectra were then

[1] Department of Astronomy, Cornell University, 610 Space Sciences Building, Ithaca, NY 14853-6801; haol@isc.astro.cornell.edu.
[2] *Spitzer* Fellow.
[3] *Spitzer* Science Center, California Institute of Technology, MS 220-6, Pasadena, CA 91125.
[4] SRON National Institute for Space Research and Kapteyn Institute, P.O. Box 800, 9700 AV Groningen, Netherlands.
[5] Department of Physics and Astronomy, University of Rochester, Rochester, NY 14627.
[6] Space Telescope Science Institute, 3700 San Martin Drive, Baltimore, MD 21218.
[7] Department of Physics, University of Crete, P.O. Box 2208, GR-71003, Heraklion, Greece.
[8] Chercheur Associé, Observatoire de Paris, 61 Avenue de l'Observatoire, F-75014 Paris, France.

[9] The IRS was a collaborative venture between Cornell University and Ball Aerospace Corporation, funded by NASA through the Jet Propulsion Laboratory and the Ames Research Center.

TABLE 1
PROPERTIES OF SOURCES

Property	PG 1351	I Zw 1	3C 273	PG 1211	PG 0804
AOR key	3760640	3761920	4978176	3760896	9074944
Date observed	2004 Apr 17	2004 Jan 7	2004 Jan 6	2004 Jan 7	2004 Mar 1
Integration time (s)	408	224	336	408	408
Redshift	0.0881	0.0611	0.158	0.0808	0.0999
Luminous distance (Mpc)[a]	398	271	749	363	455
$\log (L_{bol}/L_{\odot})$	12.14	12.20	13.44	12.44	12.56
$F_{15\,\mu m}$ (Jy)[b]	0.21	0.62	0.36	0.21	0.13

[a] Assuming $H_0 = 71$ km s^{-1} Mpc^{-1}, $\Omega_M = 0.27$, $\Omega_\Lambda = 0.73$, and $\Omega_K = 0$.
[b] Rest frame.

extracted and calibrated using the IRS standard star HR 6348 for SL and the stars HR 6348, HD 166780, and HD 173511 for LL.

After extraction, the orders were stitched, requiring order-to-order scaling adjustments of less than 5%. Finally, the stitched spectra were scaled to match the observed *IRAS* fluxes at 12 and 25 μm or IRS blue peak-up flux at 16 μm. For 3C 273, we did not attempt any scaling, since the source varies by up to 0.4 mag at 10.6 μm on timescales of up to several years (Neugebauer & Matthews 1999). The scaling factors we applied average 6%, with the largest scaling factor of 16%. The observed sources are point sources for both *IRAS* and IRS, therefore scaling to *IRAS* flux is justified. Figure 1 presents the calibrated spectra. Table 1 lists the 15 μm rest-frame fluxes.

In some spectra, most notably in I Zw 1, residual fringing due to minor pointing errors appears between 21 and 30 μm (the first order of the LL module). We have not defringed the spectra. Residual artifacts also appear in some spectra in SL order 1 (7.5–14 μm). These take the form of a roughly sinusoidal deviation from the actual spectrum and are most obvious in the spectrum of 3C 273 at 8–10 μm, where they have a maximum strength of ~3% of the total flux. Because 3C 273 has the weakest silicate emission feature in our sample, this artifact is even more pronounced in figures showing the continuum-subtracted spectra. We estimate uncertainties by comparing the spectra in the two nod positions, and these artifacts generally manifest themselves as a disagreement between the nod positions. The uncertainties only become apparent in Figures 2 and 3 shortward of 11 μm (*dark shaded area*). None of these artifacts change the conclusions reported below.

3. ANALYSIS

The spectra in Figure 1 are dominated by two broad emission features, which we identify as the Si−O stretching mode and the O−Si−O bending mode in silicate dust grains. The strength of the features is best appreciated by comparing the peak fluxes to the underlying silicate-graphite "continuum." For PG 1351, I Zw 1, and PG 1211, we define the continuum using a spline interpolation between the 5–8 μm spectrum and a point at the extreme red end of the IRS spectral range, where a change in slope indicates the end of the 18 μm silicate feature. For 3C 273 and PG 0804, the spectral structure at the red end of the IRS spectral range does not show a similar change in slope. This may indicate that dust emission is still contributing at these wavelengths. Therefore, we have assumed that the continuum at the red end runs somewhat below the observed spectrum. Figure 1 plots the resulting spline-interpolated continua (*dashed lines*), while Figure 2 shows the resulting continuum-subtracted spectra.

Comparison of the silicate emission spectra in Figure 2 reveals

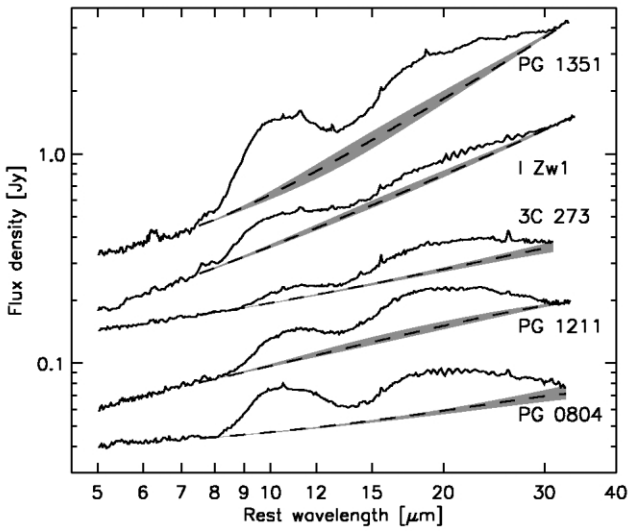

FIG. 1.—5–35 μm IRS low-resolution spectra of five PG quasars, showing silicates in emission. The pixel-to-pixel uncertainty in the data is less than 3%. Fringing effects with amplitudes of up to 5% are visible in LL order 1 (see text). For each spectrum, three choices for the silicate-graphite continuum are indicated by the dashed line and gray shaded area. The spectra have been scaled for plotting purposes, with scaling factors of 8.0 for PG 1351, 1.0 for I Zw 1, 0.77 for 3C 273 and PG 1211, and 0.50 for PG 0804.

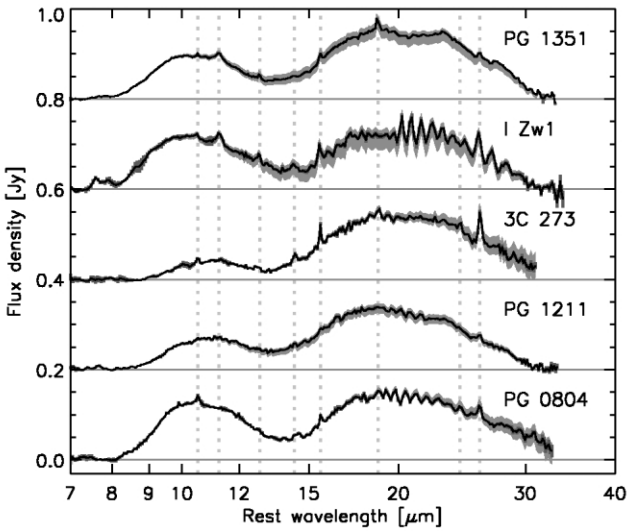

FIG. 2.—Continuum-subtracted silicate emission spectra of the five PG quasars. The spectra have been normalized and offset from each other for plotting purposes. Fringing effects are visible in LL order 1 (see text). The shaded areas indicate the uncertainty in the silicate emission spectra as introduced by the uncertainty in the observed spectrum and choice of continuum. Vertical dotted lines indicate the rest wavelengths of emission features discussed in the text.

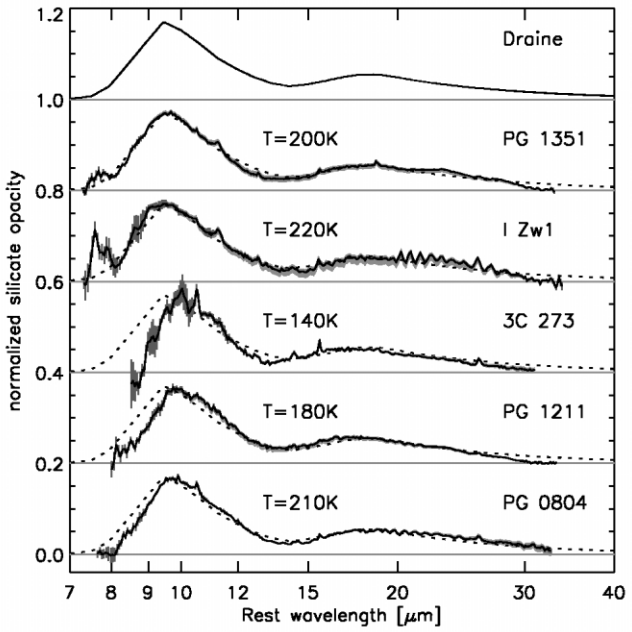

FIG. 3.—Opacity spectra for the five PG quasars compared to the scaled synthetic silicate opacity curve of Weingartner & Draine (2001) and Li & Draine (2001). The opacity spectra from the quasars are derived using the adopted silicate grain temperature and are scaled and offset for plotting purposes. The shaded areas indicate the uncertainty in the silicate profile as introduced by the uncertainty in the observed spectrum and choice of continuum.

that the ratio of the 18 and 10 μm features varies significantly within the sample. It is highest for 3C 273 and lowest for PG 0804 (see Table 2). Also, the onset and center of the shift significantly from one source to the next, and in 3C 273 and PG 1211, the 10 μm feature appears at longer wavelengths. Interestingly, these two sources happen to be the only radio-loud quasars in our sample. In order to test whether these differences can be attributed to our choice of continuum, for each source we compared the silicate emission spectra for two other choices of underlying silicate-graphite continuum: one above and one below the adopted continuum, enclosing the shaded areas in Figure 1. As illustrated by the shaded areas in Figure 2, this results in an uncertainty of up to 30% in the peak flux of the 18 μm feature and in the ratio of the 18 μm to 10 μm features. In contrast, the onset and center of the 10 μm features are not affected by different choices of continuum.

The presence of the silicate features at 10 and 18 μm allows us to estimate the mean temperature of the emitting grains by performing an unweighted χ^2 fit to the continuum-subtracted spectrum. This temperature is only physically meaningful under the assumption that the feature-emitting region is optically thin. Using the continuum-subtracted silicate opacity (see top panel in Fig. 3) derived from Weingartner & Draine (2001) and Li & Draine (2001), we force the product of a blackbody and the silicate feature opacities to fit the observed continuum-subtracted silicate features. This reduces the problem to a single free parameter, the grain temperature, and avoids concerns related to a possible nonthermal contribution to the continuum. The resulting silicate grain temperatures ($T_{\rm sil}$) range between 140 K for 3C 273 and 220 K for I Zw 1 (see Table 2). These temperatures will change by as much as 15 K, depending on the choice for the underlying silicate-graphite continuum. Uncertainties in the fitting process may amount to as much as another 10 K.

Using the derived silicate grain temperature ($T_{\rm sil}$), it is possible to compute the silicate opacity spectrum by dividing the observed silicate emission spectrum by the blackbody spectrum with temperature $T_{\rm sil}$. Figure 3 presents the resulting opacity spectra for our sample.

The top panel in Figure 3 shows the synthetic silicate opacity spectrum after subtraction of the silicate-graphite continuum component. The lower panels show the opacity spectra for the five quasars overlaid on the synthetic profile. The quasar profiles generally show good agreement at wavelengths beyond 10 μm. Below 10 μm, only PG 1351 and I Zw 1 match the synthetic profile well. In the other three spectra, the blue wing of the 10 μm band appears weak, especially in 3C 273 and PG 1211. Apart from the artifacts in the 8–10 μm region of the spectrum of 3C 273 (indicated by the large error bars in Fig. 2; see § 2) and the presence of atomic lines and PAH emission in some spectra, the 10 μm band has a smooth appearance, showing no sign of a departure from an amorphous grain structure. Evidence for some crystalline grains do appear at longer wavelengths, most notably in the spectrum of PG 1351 at 23 μm.

The weakness of the blue wing of the 10 μm silicate opacity profile in three of our sources appears to be significant and cannot be explained by the uncertainties in the observed spectrum (see the error bars in Fig. 3). Grain size and composition, geometry, optically thick radiative transfer, or a combination of these factors may explain the observed weakness. If our optically thin assumption is invalid, then the temperatures we have inferred cannot be interpreted as real dust temperatures. Jaffe et al. (2004) reported a similar deficiency in the blue wing of the 10 μm absorption feature in NGC 1068, which they attribute to a different silicate grain composition.

A close inspection of the spectra in Figures 1 and 2 reveals numerous other features. Those visible in at least one spectrum in the sample include the PAH emission features at 6.2, 7.7, and 11.2 μm, and emission lines at 10.5 μm ([S IV]), 12.8 μm ([Ne II]), 14.3 μm ([Ne V]), 15.6 μm ([Ne III]), 18.7 μm ([S III]), and 25.9 μm ([O IV]).

4. COMPARISON WITH MODELS

Direct comparisons of our observations to the predictions of published AGN radiative transfer models are difficult, given the limited resolution of model spectra in the 5–40 μm range of the IRS. Additionally, the model output is not tuned to be compared to the observed properties presented in Table 2. However, we can measure the feature-to-continuum ratio at 10 μm from the figures presented by Laor & Draine (1993), Granato & Danese (1994), Nenkova et al. (2002), and Dullemond & van Bemmel (2005). For the optically thin dust models of Laor & Draine (1993), the values range from 0.1 for models in which the grain-size distribution is dominated by larger grains to 1.5 for models with a standard grain-size distribution. In the face-on cases modeled by Granato & Danese (1994), the values range from near zero for very thick and compact configurations to 1.0 for more extended torus models. These results are similar to those by Nenkova et al. (2002) and Dullemond & van Bemmel (2005), but their highest 10 μm feature-to-continuum ratios are around 0.7 and 0.4, respectively. Given the observed range of 0.12–1.25 within our limited sample (Table 2), the model predictions for the 10 μm feature-to-continuum ratio are in good agreement. A similar comparison for the 18 μm feature-to-continuum ratio could not be undertaken, since the features are not as apparent as the 10 μm features in the AGN models.

5. DISCUSSION AND CONCLUSION

We have detected the 10 and 18 μm silicate emission features in five PG quasars—the first detection of both silicate

TABLE 2
MEASURED QUANTITIES

Parameter	PG 1351	I Zw 1	3C 273	PG 1211	PG 0804
10 μm feature-to-continuum ratio[a]	1.25	0.38	0.12	0.55	0.60
18 μm feature-to-continuum ratio[a]	0.79	0.20	0.36	0.56	0.56
18 μm to 10 μm feature ratio[a]	1.75	1.31	3.34	1.89	1.08
$F(30\ \mu\text{m})/F(5.5\ \mu\text{m})$	11.0	6.86	2.53	2.99	1.95
$L_{\rm sil}/L_{\rm bol}$	0.087	0.040	0.009	0.023	0.021
10–18 μm cont. color temperature (K)[b]	250	270	320	310	340
Silicate temperature (K)	200	220	140	180	210

[a] Evaluated at the peak of the feature.
[b] The color temperature is computed from the adopted continuum at 10 and 18 μm.

features in emission in galaxies outside the Local Group, and in AGNs in particular. Given the existence of published mid-infrared photometric and spectroscopic data for these quasars, our finding may appear surprising at first. Roche et al. (1991) obtained 8–13 μm spectra of 3C 273 and I Zw 1, but the low contrast of the silicate feature to the strong continuum, and the lack of coverage outside the *N*-band window, prevented them from identifying silicate emission. The PHT-S spectrometer on the *Infrared Space Observatory* (Lemke et al. 1996) obtained spectra of 3C 273, I Zw 1, and PG 0804 (Rigopoulou et al. 1999), but the limited wavelength coverage of PHT-S (only to 11.6 μm) and the redshifts of the quasars allowed only the blue side of the 10 μm feature to be visible. Because of these difficulties, silicate emission had remained unidentified in these five sources until now.

Our detection of silicate emission in type 1 AGNs provides support for the unified AGN model (Antonucci 1993). An AGN torus viewed pole-on should offer an unobstructed line of sight to the torus dust, the surface of which is heated to temperatures of several hundred to a thousand kelvin by the radiation from the central engine. Emission from this hot surface should produce a silicate feature in emission, under most circumstances.

Assuming a simple optically thin geometry, we find that the silicate grain temperature in our sources ranges from 140 to 220 K, which is well below the dust sublimation temperature. A detailed comparison of the derived opacity profiles for our quasars indicates that our simple model cannot satisfactorily explain the absence of a blue wing in the 10 μm feature for three of our quasars. This likely points to a more complex geometry involving radiative transfer within a (partially) optically thick environment—probably an AGN torus. It may also point to differences in the grain size or composition. Our derived silicate grain temperatures should therefore only be used as a characterization of the observed spectra, not as a means to infer the actual temperature and geometry of the AGN.

From our limited sample of PG quasars (three, in addition to the sample discussed in this Letter) and a few Seyfert 1 galaxies, it is clear that 10 μm silicate emission is not a ubiquitous feature in mid-infared spectra of type 1 AGNs. Only five out of 12 continuum-dominated AGNs show this feature prominently. Interestingly, the quasars that show a 10 μm silicate emission feature all have bolometric luminosities higher than $10^{12}\ L_{\odot}$, while the other type 1 AGNs are less luminous. Models that can explain the presence of the 10 μm silicate emission feature in some type 1 AGNs will also need to explain their absence in others.

The authors wish to thank Bill Forrest, Elise Furlan, and Terry Herter for their useful discussions. Support for this work was provided by NASA through contract 1257184, issued by the Jet Propulsion Laboratory, California Institute of Technology, under NASA contract 1407. H. W. W. S. was supported under this contract through the *Spitzer Space Telescope* Fellowship Program.

REFERENCES

Antonucci, R. 1993, ARA&A, 31, 473
Antonucci, R. R. J., & Miller, J. S. 1985, ApJ, 297, 621
Armus, L., et al. 2004, ApJS, 154, 178
Boroson, T. A., & Green, R. F. 1992, ApJS, 80, 109
Dullemond, C. P., & van Bemmel, I. M. 2005, A&A, in press (astro-ph/0501570)
Efstathiou, A., & Rowan-Robinson, M. 1995, MNRAS, 273, 649
Genzel, R., et al. 1998, ApJ, 498, 579
Granato, G. L., & Danese, L. 1994, MNRAS, 268, 235
Houck, J. R., et al. 2004, ApJS, 154, 18
———. 2005, ApJ, 622, L105
Jaffe, W., et al. 2004, Nature, 429, 47
Knacke, R. F., & Thomson, R. K. 1973, PASP, 85, 341
Laor, A., & Draine, B. T. 1993, ApJ, 402, 441
Lemke, D., et al. 1996, A&A, 315, L64
Li, A., & Draine, B. T. 2001, ApJ, 554, 778
Nenkova, M., Ivezić, Ž., & Elitzur, M. 2000, in ASP Conf. Ser. 196, Thermal Emission Spectroscopy and Analysis of Dust, Disks, and Regoliths, ed. M. L. Sitko, A. L. Sprague, & D. K. Lynch (San Francisco: ASP), 77
Nenkova, M., Ivezić, Ž., & Elitzur, M. 2001, in ASP Conf. Ser. 247, Spectroscopic Challenges of Photoionized Plasmas, ed. G. Ferland & D. W. Savin (San Francisco: ASP), 383
———. 2002, ApJ, 570, L9
Neugebauer, G., & Matthews, K. 1999, AJ, 118, 35
Pier, E. A., & Krolik, J. H. 1992, ApJ, 401, 99
———. 1993, ApJ, 418, 673
Rigopoulou, D., Spoon, H. W. W., Genzel, R., Lutz, D., Moorwood, A. F. M., & Tran, Q. D. 1999, AJ, 118, 2625
Roche, P. F., Aitken, D. K., Smith, C. H., & Ward, M. J. 1991, MNRAS, 248, 606
Sanders, D. B., Phinney, E. S., Neugebauer, G., Soifer, B. T., & Matthews, K. 1989, ApJ, 347 29
Siebenmorgen, R., Haas, M., Krügel, E., & Schulz, B. 2005, A&A, in press (astro-ph/0504263)
Spoon, H. W. W., et al. 2004, ApJS, 154, 184
Tran, Q. D. et al., 2001, ApJ, 552, 527
van Bemmel, I. M., & Dullemond, C. P. 2003, A&A, 404, 1
Weingartner, J. C., & Draine, B. T. 2001, AJ, 548, 296
Werner, M. W., et al. 2004, ApJS, 154, 1